

Proceedings of the Fourteenth International Conference on
Computational Structures Technology
Edited by B.H.V. Topping and J. Kruis
Civil-Comp Conferences, Volume 3, Paper 14.1
Civil-Comp Press, Edinburgh, United Kingdom, 2022, doi: 10.4203/ccc.3.14.1
©Civil-Comp Ltd, Edinburgh, UK, 2022

Flexural Behavior of Ferrocement Cold-Formed Hollow Steel Composite Beams

E. Elkassas, A. M. Morsy and M. Marzouk

**Construction and Building Engineering Department, AASTMT,
Alexandria, Egypt**

Abstract

Experimental and numerical studies are carried out to investigate the flexural behavior of precast lightweight composite beams. This composite beam is comprised of a slender cold-formed hollow section of dimension (140x180 mm) with different thicknesses surrounded by a ferrocement layer. This composite beam is called a precast ferrocement cold-formed hollow section (FCH). The main problem in this study is the local buckling of cold-formed hollow sections before reaching yield. The objective of these studies is to examine the flexural behavior of precast ferrocement cold-formed composite beams with and without shear connectors. Nine beams with a span of 1500 mm were tested under a four-point bending system to evaluate their flexural strength. Four different parameters have been examined, which are the spacing of shear connectors, ferrocement thickness, and hollow steel section thickness. The test results showed that the presence of a 30 mm ferrocement layer increased the capacity by 18% when compared with the control specimen. The presence of shear connectors increases the capacity by 30%. Increasing the steel cross-section thickness leads to an increase in the capacity by 16-33% and finally, increasing the surface friction has a very small effect on the section capacity, which can be neglected. The finite element models were developed and validated by the test results. The results show a close agreement between the experimental and finite element results. Extensive parameters were investigated, which were mortar compressive strength (f'_c) and the position of shear connectors. The results indicated that increasing mortar strength leads to an increase in section capacity ranging between 11% and 18%. The presence of a shear connector in the web and the lower flange of the hollow section have a very small effect.

Keywords: cold-formed steel, ferrocement, composite beam, local buckling, precast, shear connector

1 Introduction

In recent years, composite steel-concrete structural systems have become a popular design and construction technique. In comparison to traditional reinforced concrete beams, composite steel-concrete beams have numerous advantages, including lighter steel weight, longer span, and faster erection. As the world's steel industry transitions from hot-rolled sections and plates to coil and strip, cold-formed steel (CFS) products are becoming more commonly employed in structural design. There are many shapes of cold-formed. This study focused on cold-formed hollow steel sections. Cold-formed hollow sections are now permitted in all major structural design standards such as AISC 360-16 [1], BS 5950 [2], AS 4100 [3], and EC3 2004 [4].

The use of a thin wall plate in the hollow section can lead to flexural and local buckling failure, as described by Jouaux [5]. Design codes classify hollow steel sections into compact, non-compact, and slender sections based on their bending behavior. Design codes define compact sections as those that can reach plastic moments without local buckling, non-compact sections as those that can reach yield moments without local buckling, and slender sections as those that cannot reach yield moments due to local buckling. AISC 360-16 [1] gives a slender limit for classifying hollow sections. The flange is considered compact when the slender ratio (b/t) is less than $(1.12\sqrt{E/f_y})$ and non-compact when it is less than $(1.40\sqrt{E/f_y})$. The web is considered compact when the slender ratio (h/t) is less than $(2.42\sqrt{E/f_y})$ and non-compact when it is less than $(5.70\sqrt{E/f_y})$. This study focused on the slender sections, with flange slender limits ranging from 43 to 67 calculated according to AISC 360-16 [1].

Ferrocement is a Ferro (iron) and cement mortar composite. Ferrocement is a type of thin-walled reinforced concrete in which wire mesh layers are distributed uniformly throughout the matrix. The ACI 549 committee [6] explained that ferrocement is a type of reinforced concrete that behaves differently than conventional reinforced concrete in which the reinforced elements are dispersed throughout the matrix. According to the ACI Committee, the ferrocement matrix consists of fine sand passed through sieve ASTM No. 8 (2.36 mm), with a sand-cement ratio by weight ranging from 1.5 to 2.5 and a water-cement ratio ranging from 0.35 to 0.5. Naaman [7] outlined the mechanical properties of ferrocement. According to Naaman, ferrocement has homogenous isotropic properties in two directions, high tensile strength that is of the same order as its compressive strength, high reinforcement ratio, and good durability under environmental exposures.

Researches on the structure behavior of composite sections comprised of concrete and cold-formed steel have been conducted. Alhajri [8] et al. outlined experimental and numerical studies to examine the structural behavior of nine precast U-shaped composite beams. The study investigated the effect of the number of wire mesh and thickness of steel sections on structural behavior. The test results demonstrated that increasing the number of wire mesh, as well as the steel thickness, led to an increase in section capacity. Cheng-Tzu Thomas Hsu [9] et al. studied an experimental study

of new composite beams to investigate their structural behavior. These composite beam were comprised of a reinforced concrete slab on a corrugated cold-formed metal deck, back-to-back cold-formed steel joists, and a continuous cold-formed furring shear connector. The study investigated the maximum moment capacity and deflection of specimens. The test results indicated that that the composite beams can reach its ultimate capacity without buckling due to this type of shear connector. El-Sayed [10] et al. presented an experimental study to investigate the structural behavior of a cold-formed square hollow column section strengthened by mortar under compression. The study examined the effect of the thickness of polymer mortar on the capacity of the column.

In this study, a new type of a precast lightweight composite beam was comprised of a slender cold formed hollow section (CFS) strengthened by a ferrocement layer called a precast ferrocement cold-formed hollow steel section (FCH). This system could provide an alternative composite system for floor and roof in medium and small size buildings. The main problem of slender hollow sections is local buckling before reaching yield. The objective of this study is to investigate the flexural behavior of a precast composite beam by performing experimental tests and finite element analysis.

2 Methods

2.1 Experimental program

Nine simply supported beams were tested. The aim of the tests was to study the flexural behavior and the strength of a ferrocement encased cold-formed hollow steel beam with different parameters and to validate the numerical analysis. A four-point bending system is used in these tests. All specimens were 1800 mm long and spanned 1500 mm between the supports. Figure 1 shows the specimen's details. Four parameters were studied in these tests. The first parameter is the spacing of the shear connectors, which are (100, 200, and 300 mm), where bolts of diameter 6 mm and length of 25 mm are used as shear connectors with grade (8.8) as shown in Figure 2. The second parameter is ferrocement thickness, which are (30 mm, and 50 mm). The third parameter is cold-formed steel thickness, where (2, 2.5 and 3 mm) are studied. The fourth parameter is the effect of surface friction where diamond plates are used to be compared with ordinary smooth plates, Figure 3 shows the diamond plate shape. Table 1 summarizes the specimen's details. All specimens were reinforced with one layer of welded wire mesh of a grade (St. 37) of diameter 1.5 mm surrounds the hollow steel beams as shown in Figure 4. All cold-formed hollow steel sections in this study are un-galvanized with grade (St. 37) as indicated by manufactured. Figure 5 shows the hollow steel section dimensions. The mortar matrix comprised of ordinary Portland cement and sand passing though ASTM No. 8 (2.36 mm), free from any deleterious material. The mix proportion of sand/cement was 2/1 by weight, and with a water-cement ratio of 0.5. The compressive strength of the mortar according to ACI 549 [6] on day 28 is 23 N/mm². Test specimens were supported with roller and pinned supports, so that they were simply supported beams. The deflections of specimens were recorded by dial gauge at mid-span. Strain gauges were installed at the top and

bottom of the hollow steel sections at mid-span to evaluate the stress-strain curves. Figure 6 shows the loads and instrumentation set-up.

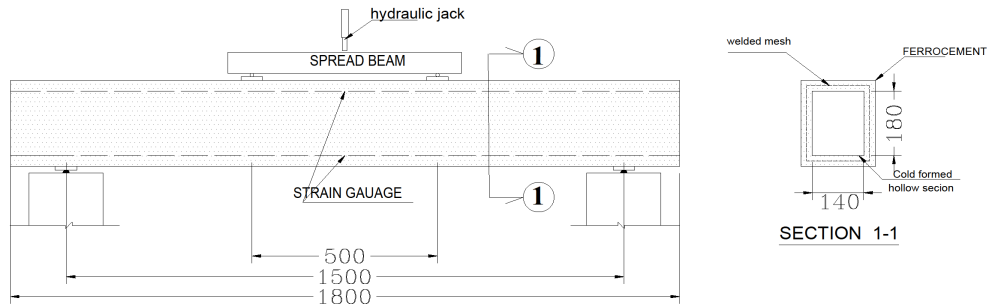


Figure 1: Specimen details.

| Specimens ID | Mortar thickness (mm) | Steel thickness (mm) | Shear connector Spacing (mm) |
|----------------|-----------------------|----------------------|------------------------------|
| CONTROL | - | 2.5 | - |
| FCH1 | 30 | 2.5 | 100 |
| FCH2 | 30 | 2.5 | 200 |
| FCH3 | 30 | 2.5 | 300 |
| FCH4 | 30 | 2.5 | N/A |
| FCH5 | 50 | 2.5 | N/A |
| FCH6 | 50 | 2 | N/A |
| FCH7 | 50 | 3 | N/A |
| FCH8 | 50 | 2 -(Diamond sheet) | N/A |

(N/A) denote to without shear connector.

Table 1. Specimen's details.

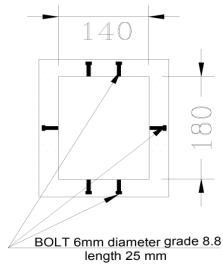


Figure 2: Shear connector's positions



Figure 3: Diamond plate shape.



Figure 4: Welded wire mesh.

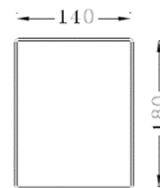


Figure 5: Cold-formed hollow section dimensions.

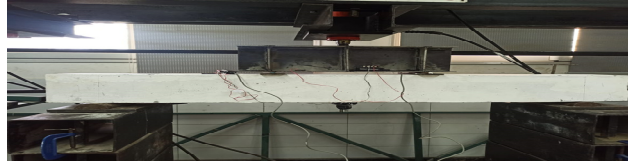


Figure 6: Load and instrumentation set up.

2.2 Numerical analysis

Numerical investigation were performed on nine simply supported beams. For numerical study, finite element models have been developed to investigate the behavior of precast composite beams. Ansys Mechanical APDL V19 software was used to create the F.E models. Figure 7 shows the finite element model. The models are built through the following steps: (a) geometric model using suitable elements, (b) material assignment, and (c) load and boundary conditions.

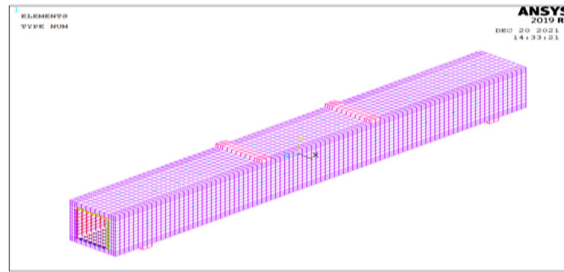


Figure 7: Finite element model details.

2.2.1 Geometric model

The accuracy of finite element models depends on the selection of the suitable elements to predict the real behavior of members. These elements are mainly classified based on the features embedded in the element type. In this study, four different types of elements were used. The cold-formed section is modeled using a 4-node shell element (SHELL181) as shown in Figure 8. The Ferrocement is modeled using an 8-node element (SOLID65) as shown in Figure 9. This element has the capability of plastic deformation, cracking in three orthogonal directions, and crushing. The following three techniques, which are shown in Figure 10 are used to model steel reinforcement as described by Azimi et al. [11], which are (a) discrete model, (b) embedded model, and (c) smeared model. In this study, wire mesh is modeled by a smeared model. The steel wire meshes were defined by the volume fraction, orientation angle, and initial strain. The normal and dowel stiffness of shear connector behavior is simulated by two element. The normal forces transmitted by the axial forces in the shear connectors are represented in the ANSYS model by the link element (LINK180), while, the shear forces that are resisted by the shear connectors are represented by a nonlinear spring element (COMBIN39). The load-slip

relationship value for the nonlinear spring element (COMBIN39) was determined according to Equation (1) which is presented by (Lorene and Kubica) [12]. Figure 11 and Figure 12 shows LINK180 and COMBIN39 geometries. The contact surface between the ferrocement and the hollow section was simulated by (CONTA174 and TARGE170) elements.

$$\frac{P}{P_u} = (1 - e^{-0.55S})^{0.3} \quad (1)$$

Where P_u is stud shear capacity, which is determined by ANSI/AISC 360-05 [1].

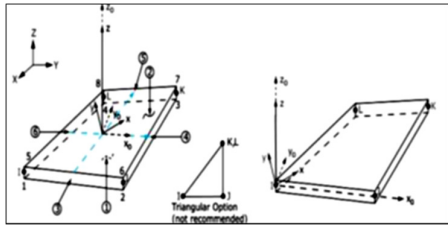


Figure 8: SHELL 181 geometry, ANSYS.

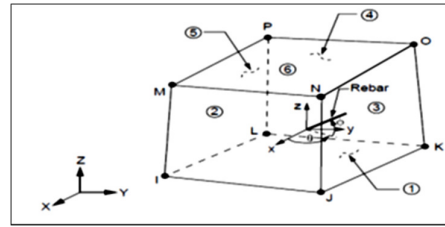


Figure 9: Solid65 geometry, ANSYS

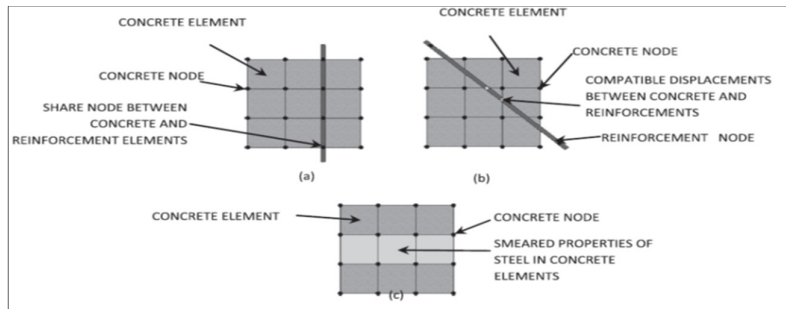


Figure 10: Reinforced modeling techniques (a) discrete model, (b) Embedded model and (c) smeared mode.

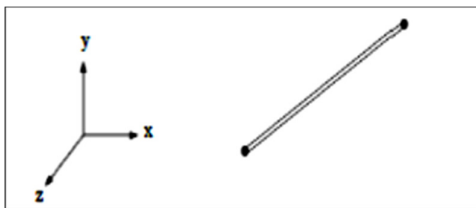


Figure 11: Link 180 geometry, ANSYS.

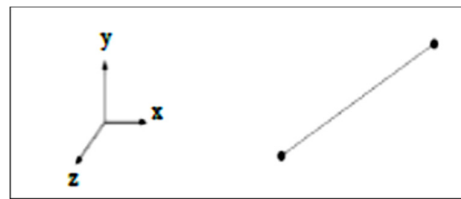


Figure 12: Combin39 geometry, ANSYS.

2.2.2 Material

The nonlinear properties of the mortar under compression, as shown in Figure 13, are assigned to develop F.E models throughout the defining of stress-strain relations

which is developed by Desayi and Krishnan [13] through the Equation (3) and Equation (4). The properties of steel are assumed to be isotropic, elastic-perfectly plastic, which behaves identically in tension and compression with stiffness only in the axial direction.

$$F_c = \frac{\varepsilon_c E_c}{1 + \left(\frac{\varepsilon_c}{\varepsilon_0}\right)^2} \quad (2)$$

$$\varepsilon_0 = \frac{2F_c}{E_c} \quad (3)$$

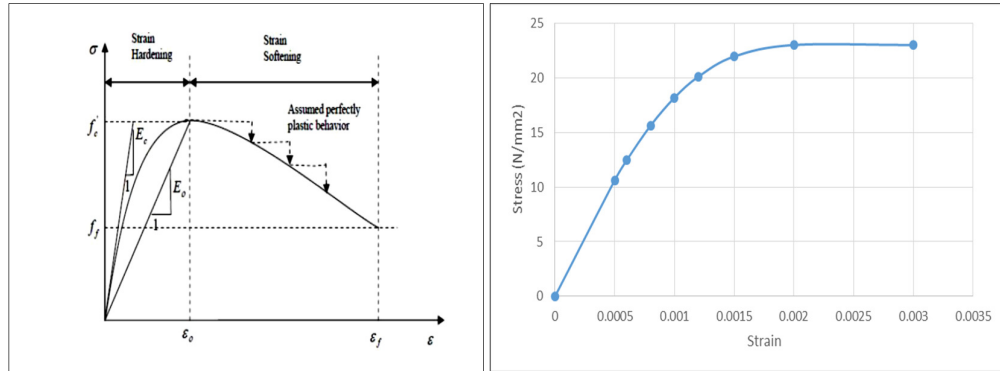


Figure 13: Stress-Strain curve under compression.

3 Results

3.1 Test results

Experimental results in terms of failure load, ultimate moment, and mode of failure of all specimens are tabulated in Table 2. It was found that the presence of a 30 mm ferrocement layer without shear connectors increases the capacity by 18% when compared with the control specimen due to composite action. The presence of shear connectors in specimens (FCH1, FCH2, and FCH3) increased the section capacity by 26% compared with (FCH4) (without shear connector). The mortar thickness was studied in specimens (FCH4 and FCH5). It can be seen that the capacity of the section increased by 31% when mortar was increased from 30 mm to 50 mm. The steel thicknesses were investigated using specimens (FCH5, FCH6, and FCH7). It can be seen that increasing thickness has a significant effect on the structural behavior of a composite section. Increasing the thickness from 2 to 2.5 mm-increased section capacity by 29%, while increasing the thickness from 2 to 3 mm increased the capacity by 40%. The increase in surface friction by using diamond plates is being studied. It can be noticed that the change of plate type from ordinary to diamond plate with the same thickness has an insignificant effect on the structural behavior and on the buckling behavior of steel sections, which can be neglected. The failure modes observed can be classified into two types: mortar crushing followed by buckling hollow section or buckling hollow section only. Figure 14 shows the (FCH1 and FCH5) failure mode. No slip between the ferrocement and hollow section was noticed, as shown in Figure 15. It was noticed that shear connectors experienced little deformation.

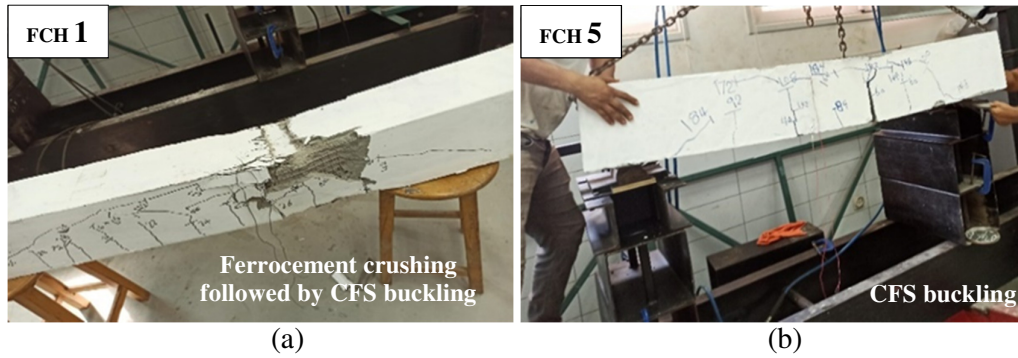


Figure 14: FCH1 and FCH5 failure modes.

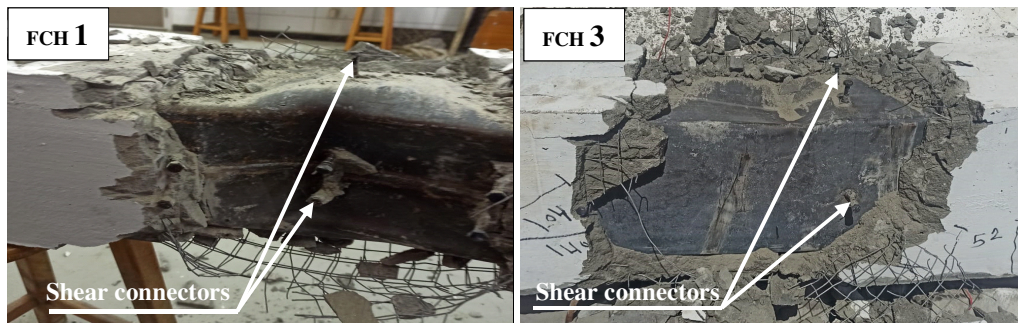


Figure 15: FCH1 and FCH3 shear connectors after test.

| Specimens ID | Failure load (Pu) kN (EXP.) | Mode of failure |
|--------------|-----------------------------|---|
| CONTROL | 110 | CFS buckling |
| FCH1 | 164 | FerroceMENT crushing followed by CFS buckling |
| FCH2 | 164 | FerroceMENT crushing followed by CFS buckling |
| FCH3 | 165 | FerroceMENT crushing followed by CFS buckling |
| FCH4 | 130 | CFS buckling |
| FCH5 | 170 | CFS buckling |
| FCH6 | 132 | CFS buckling |
| FCH7 | 185 | CFS buckling |
| FCH8 | 136 | CFS buckling |

Table 2: Experimental results.

3.2 Finite element result

3.2.1 Verification

Finite element models were developed and validated by the test results. Comparison was made for failure load (P_u), mid span deflection and crack patterns. Figure 16 shows the results obtained from the experimental data and were compared with

outputs from finite element models. The ratio between the results of failure load obtained from both the experimental test (P_{EXP}) and ANSYS (P_{FEM}) was then calculated for all specimens and is tabulated in Table 3. The finite element and experimental cracks for specimen FCH1 are shown in Figure 17. The results show a close agreement between the experimental and finite element results. Therefore, finite element models established in this study can accurately predict the load versus deflection response and failure modes.

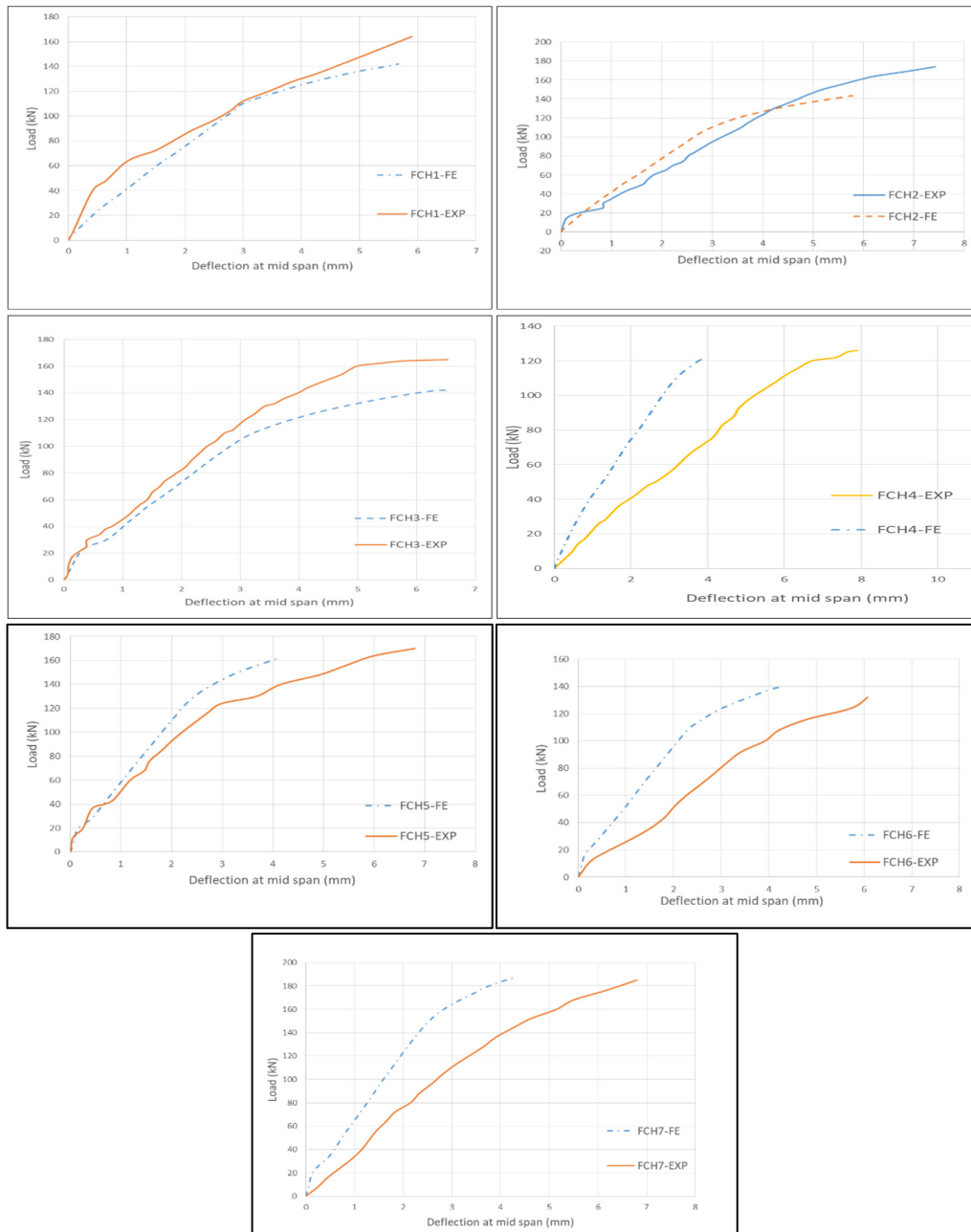


Figure 16: Experimental and finite element comparison.

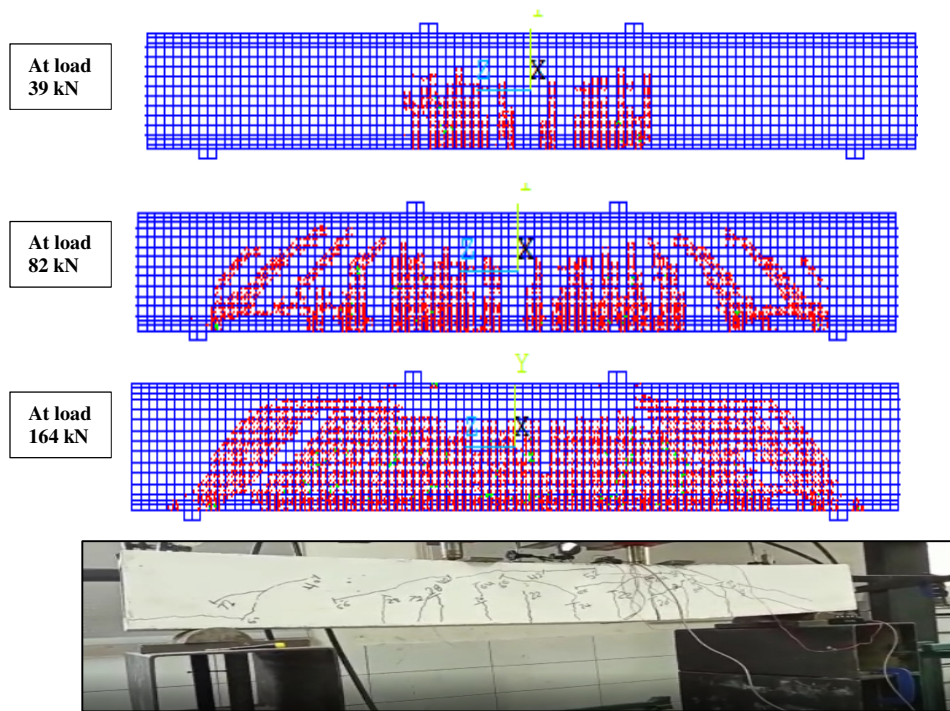


Figure 17: FCH1 specimen cracks pattern.

| Specimens ID | Failure load (Pu) kN FEM. | Failure load (Pu) kN EXP. | $(P_u)_{EXP} / (P_u)_{FINITE}$ | Max. Deflection at mid span (mm) EXP. | Max. Deflection at mid span (mm) FEM. |
|--------------|---------------------------|---------------------------|--------------------------------|---------------------------------------|---------------------------------------|
| FCH1 | 142 | 164 | 1.15 | 5.9 | 5.67 |
| FCH2 | 142 | 164 | 1.15 | 7 | 5.77 |
| FCH3 | 142 | 165 | 1.15 | 6.5 | 6.5 |
| FCH4 | 121.5 | 130 | 1.07 | 7.9 | 4.5 |
| FCH5 | 161.5 | 170 | 1.052 | 6.8 | 4.1 |
| FCH6 | 139.5 | 132 | 0.946 | 6.1 | 4.25 |
| FCH7 | 186 | 185 | 0.99 | 6.8 | 4.25 |

Table 3: Experimental and finite element results.

3.2.2 Parametric study

Parametric studies were conducted using the finite element method to investigate the effects of hollow steel section thickness, mortar compressive strength (f'_c), and the location of the shear connectors on the flexural behavior of the composite beam.

Influence of CFS thickness on composite beam capacity

To obtain the effect of cold-formed hollow section thickness (CFS) on the composite beam capacity, six FE models with CFS thicknesses (0.5, 1, 1.5, 2, 2.5, and 3) were analysed. The hollow section dimensions are 180x140 mm and the mortar thickness is 50 mm without a shear connector. A failure load-CFS thickness graph is shown in Figure 18. It can be seen that as the thickness increases, the failure load increases and stiffness increases.

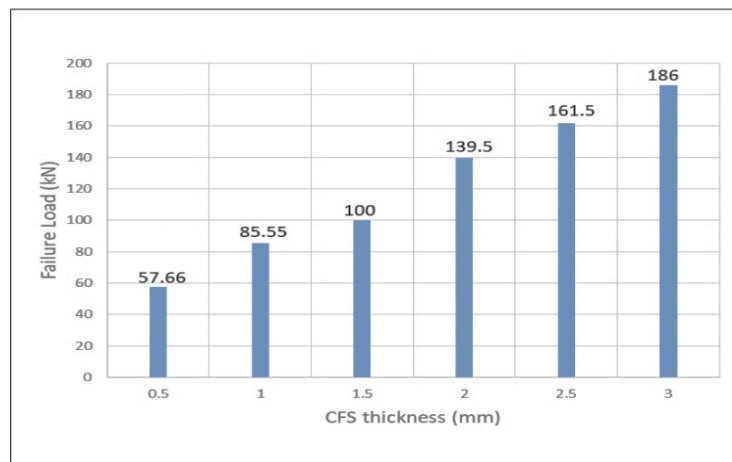


Figure 18: Failure load – CFS thickness graph.

Influence of location of shear connector

To investigate the effect of the location of shear connectors, three models were investigated with a different location for the shear connector as shown in Figure 19. The spacing of shear connectors for three models is (100 mm). It was found that using two bolts in the upper flange of the hollow section has a very small effect on section capacity when compared with one bolt in middle. The presence of bolts in the web and lower flange of the hollow section also has a very small effect. Load versus mid-span deflection curves are shown in Figure 20.

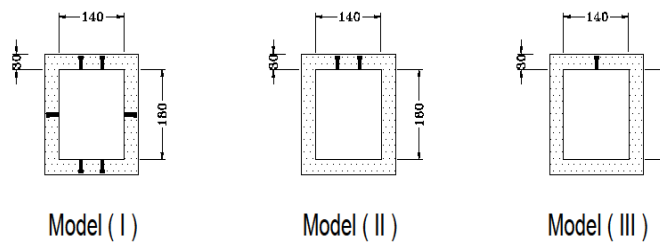


Figure 19: Shear connector location.

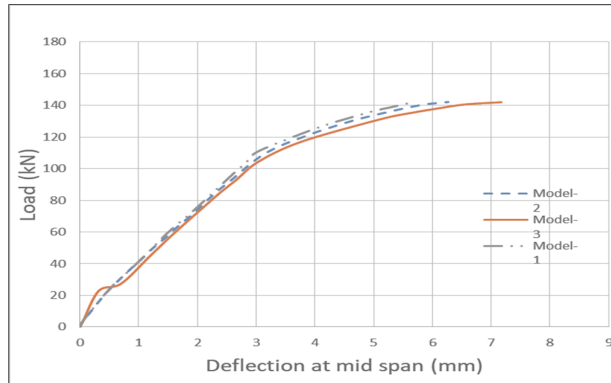


Figure 20: Failure load – CFS thickness curve.

Influence of mortar compressive strength (f'_c)

Three finite element models with mortar compressive strengths of (23, 40, and 50 MPa) were established to study the effect of concrete compressive strength on composite beam capacity. The section dimensions, CFS thickness, and shear connector spacing are the same as the specimen (FCH1). Load versus mid-span deflection curves are shown in Figure 21. It can be seen that section capacity increased by 11 % when mortar compressive strength increased from (23 to 40 MPa) and by about 18 % when compressive strength increased from (23 to 50 MPa).

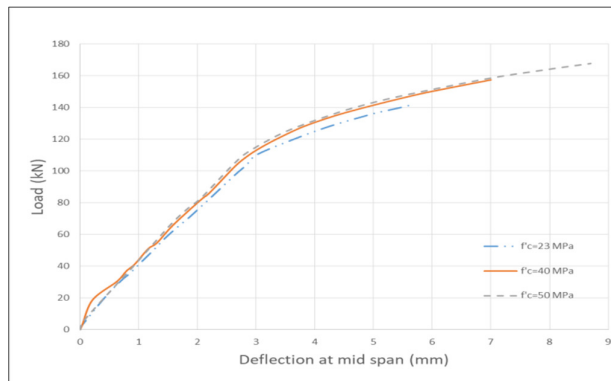


Figure 21: Load vs. mid-span curves.

4 Conclusions and Contributions

Based on experimental and numerical results and observations for the nine specimens, the following conclusions can be drawn:

1. The presence of mortar of a thickness of 3 cm increases section capacity when compared with steel hollow section capacity of dimension (180x140x2.5 mm) by about 15% due to composite action.
2. Shear connectors increase section capacity by about 30% as they delay local buckling until compression failure of mortar.

3. Increasing mortar thickness leads to an increase in section strength by about 31% due to the increase of the compression zone.
4. The increase in steel thickness section leads to an increase in section capacity ranging from 29% to 40%.
5. The increase in friction between mortar and hollow section caused by using diamond plate has a very small effect on section capacity, which can be neglected.
6. The increase in mortar compressive strength led to an increase in section strength range of 11% to 18%.
7. The effect of the spacing of shear connectors on section capacity is very small, which can be neglected.

References

- [1] ANSI/AISC 360-10, Specification for structural steel buildings, Chicago, USA: American Institute of Steel Construction (AISC), 2016.
- [2] BS5950-1, Structural use of steelwork in building: Code of practice for design, London, England: British Standards Institution, 2000.
- [3] AS/NZS4600, Cold-formed steel structure, Sydney, Australia: Standards Australia/Standards New Zealand, 2005.
- [4] EN 1993-1-1, Design of steel structures–Part 1.1: general rules and rules for buildings, Brussels, Belgium: European Committee for Standardization, 2005.
- [5] R. Jouaux, "The plastic behavior of cold-formed SHS (square hollow sections) under bending and compression," Diploma Thesis, Department of Civil Engineering, 2004.
- [6] ACI Committee 549-1R-88, Guide for design construction and repair of ferrocement, ACI 549-1R-88 and 1R-93 manual of concrete practice, Detroit, 1993.
- [7] A. E. Naaman, Ferrocement and Laminated Cementitious Composites, Ann Arbor, Michigan, USA: Techno Press 3000, 2000.
- [8] T. M. Alhajri, M. M. Tahir, M. Azimi, M. M. Lawan, K. K. Alenezi, M. B. Ragaee, "Behavior of pre-cast U-Shaped Composite Beam integrating cold-formed steel with ferro-cement slab," *Thin-Walled Structures*, vol. 102, pp. 18-29, 2016.
- [9] CT. Hsu, S. Punurai, W. Punurai, Y. Majdi , "New composite beams having cold-formed steel joists and concrete slab," *Engineering Structures*, vol. 71, p. 187–200, 2014.
- [10] K. M. El-Sayed, A. S. Debaiky, N. K. Nader, I. M. El-Shenawy, "Improving buckling resistance of hollow structural steel columns strengthened with polymer-mortar," *Thin-Walled Structures*, vol. 137, p. 515–526, 2019.
- [11] M. Azimi, A. Bin Adnan, M. Tahir, A. R. Sam, Sk. Abd Razak, "Seismic performance of ductility classes medium RC beam-column connections with continuous rectangular spiral transverse reinforcements," *Lat. Am. J. Solids Struct*, vol. 12, no. (4), p. 787–807., 2015.
- [12] W. Lorenc, E. Kubica, "Behavior of composite beams pre-stressed with external tendons," *J. Constr. Steel Res.*, vol. 62, pp. 1353-1366, 2006.
- [13] P. Desayi, S. Krishnan, "Equation for the Stress-Strain Curve of Concrete," *Journal of the American Concrete Institute*, vol. 61, pp. 345-350, 1964.